Stacking Lanthanide-MOF Thin Films to Yield Highly Sensitive Optical Thermometers

Dong-Hui Chen,* Ritesh Haldar, and Christof Wöll

ABSTRACT: Easy-to-integrate, remote read-out thermometers with fast response are of huge interest in numerous application fields. In the context of optical read-out devices, sensors based on the emission of lanthanides (Eu(III), T b(III)) are particularly promising. Here, by using a layer-by-layer (LbL) approach in the liquid-phase epitaxy process, a series of continuous, low-thickness lanthanide-MIL-103 SURMOFs were fabricated to yield highly sensitive thermometers with optical readout. These Ln-SURMOFs exhibit remarkable temperature-sensing photoluminescence behavior, which can be read out using the naked eye. High transmittance is realized as well by precisely controlling the film thickness and the quality of these Ln-SURMOF thermometers. Moreover, we demonstrate that the thermal sensitivity can be improved in the temperature regime above 120 K, by controlling the energy transfer between Tb(III) and Eu(III). This performance is achieved by employing a sophisticated supramolecular architecture, namely MOF-on-MOF heteroepitaxy.

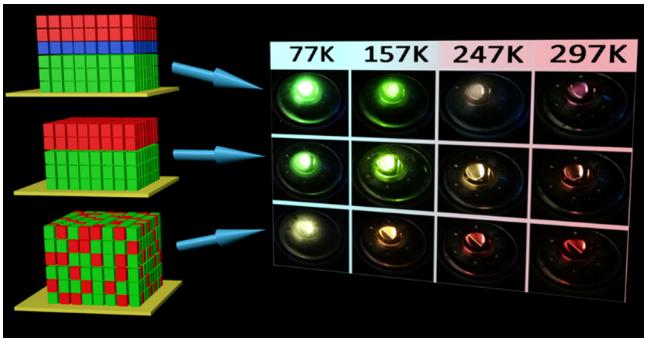

KEYWORDS: *heterostructure, lanthanide metal−organic frameworks, thermometer, energy transfer, thin film*

INTRODUCTION

Precise and rapid temperature-sensing with contactless readout is a key requirement in science and engineering.[1−4] In a continuous effort to improve the performance of such devices, advanced materials and technologies are being developed for applications in various fields, including the monitoring of industry reactions and biological processes, as well as in cryogenics technology.[5−7] In this context, temperature sensors with optical readout are of particular interest, since they allow for straightforward integration without the need for electrical contacts. Among the different variants of optical temperature sensors, luminescence-based devices have particularly appealing properties.[5,8,9] Appropriate choice of materials allows to determine the temperature directly from the ratio of two emitted intensities.[10−12]

Lanthanide-based compounds, where chromophoric antennas are attached to the metal ions, are very attractive in this context. The excitations resulting from light absorption in the antennas is transferred to the metal centers, where recombination leads to the emission of photons with characteristic frequencies.[13−16] If the energy differences between the antenna excited $\pi^*-\pi$ state and the Ln exited states are sufficiently low, thermal activation can result in a back-transfer, thus rendering a temperature dependence to the Ln emission intensities.[17−22] Ratiometric combination of two different lanthanides (e.g., Tb(III), Eu(III)) then allows, after a suitable calibration, the determination of temperature from the ratio of the two characteristic Ln emissions. Ratiometric thermometers based on this strategy have been reported in earlier studies.[23−28]

Evidently, for obtaining devices with reproducible performance and predictable dependence of the emission ratio on temperature, a precise control of mixing of the lanthanide centers is crucial. In this context, the uncontrollable, direct energy transfer between Ln ions limits performance. Simple mixing of appropriate compounds allows only for limited control of the Ln−Ln distances. Therefore, crystalline metal−organic frameworks (MOFs), where the lanthanide ions are connected by appropriately functionalized chromophores acting as linkers, are very well suited for the fabrication of Ln-based sensor materials.[29−31] The virtually infinite number of different chromophoric linkers allows easy tuning of light absorption and energy transfer.[32−34] These features of lanthanide-based MOFs have been well explored to make luminescent sensors and thermometers.[11,19,35]

A remaining problem is the distribution of the two different lanthanides in the MOF. When using a simple mixture of the

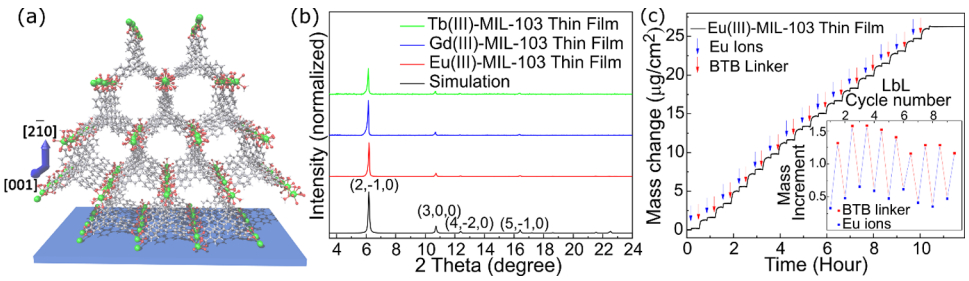

Figure 1. (a) Schematic illustration of Ln(III)-MIL-103 thin films (Ln = Eu(III), Tb(III) or Gd(III)), the substrate with the functionalized surface is simplified as blue slice; (b) out-of-plane XRD patterns of the Eu(III)-MIL-103 thin film, Tb-(III)-MIL-103 thin film and Gd(III)-MIL-103 thin film; (c) mass change per square centimeter during the LbL growth of Eu(III)-MIL-103 thin film measured by a quartz crystal microbalance (QCM), inset: mass change in each step.

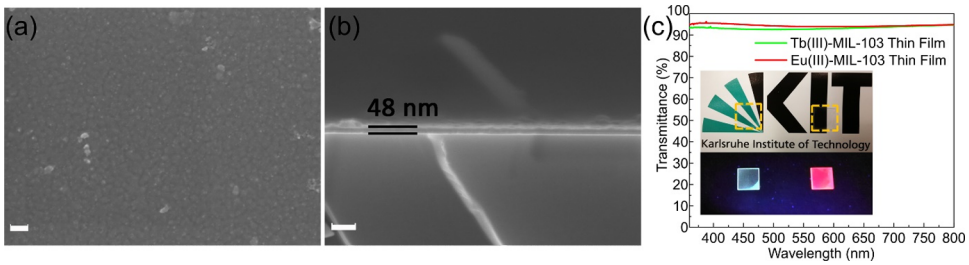

Figure 2. (a) Top view of Eu(III)-MIL-103 thin film (40 layers), the length of the white scale bar is 200 nm; (b) cross-section of Eu(III)-MIL-103 thin film (40 layers), the length of the white scale bar is 200 nm; (c) UV−visible transmittance spectra of Eu(III)-MIL-103 thin film (red) and Tb(III)-MIL-103 thin film (green) in visible light range, inset: photographs of Eu(III)-MIL-103 thin film (right) and Tb(III)-MIL-103 thin film (left) under sunlight (top) and 285 nm ultraviolet light (bottom).

two different lanthanides, often segregation occurs during the solvothermal MOF synthesis, leading to strongly varying emission rations upon illumination.[36] For a homogenous mixing of, e.g., Tb(III) and Eu(III) the above-mentioned, uncontrollable energy transfer leads to a substantial decrease of the Tb(III) emission. If segregation occurs, this unfavorable effect will be reduced.[10,37,38] As a consequence, the rational adjustment of luminescence color and temperature sensitivity depends very sensitively on the synthesis parameters and is difficult to predict.

In principle, these problems can be overcome when instead of the conventional solvothermal MOF synthesis a layer-by-layer (LbL) scheme is used to fabricate MOF thin films.[34,39,40] In this work, we have explored the LbL growth approach to create heterolayers of lanthanide MOFs and demonstrated its superior performance as a thermometer with substantially improved sensitivity.

LbL, liquid-phase epitaxial growth has been applied before to grow oriented, transparent thin films of lanthanide-based MOF-76.[41,42] Precise thickness control and heteroepitaxial growth of the Tb(III) and Eu(III) MOF-76 allowed tuning the emission color in a predictive fashion, whereas for Tb(III)-Eu(III) mixed-MOF-76 fabricated using mixtures, large fluctuations were observed. In this work, we have explored a new lanthanide-MOF, Ln-BTB (BTB = 1,3,5-tris (4-carboxy phenyl) benzene) or MIL-103.[43−45] We have synthesized thin films of MIL-103 with Eu(III), Tb(III), and Gd(III) metal ions using the LbL methodology. Control over the thickness of the individual Ln(III) MOFs allowed us to grow heterolayer MOFs with strongly reduced inter-Ln(III) energy transfer rates. We demonstrated that this approach of heterolayer fabrication yields a highly sensitive luminescent thermometer with a straightforward optical read-out.

RESULTS AND DISCUSSION

The present work is based on a lanthanide (Ln)-based MOF, also known as MIL-103, constructed by connecting Ln (Eu(III), Tb(III), Gd(III)) ions via 1,3,5-benzenetrisbenzoate (BTB) linkers. In MIL-103, 9-fold coordinated Ln(III) ions [LnO_9] form a chain running along the crystallographic [001] direction.[43−45] These chains are connected by BTB linkers to yield channels with a hexagonal cross-section (10 × 10 Å^2), as illustrated in Figure 1a. The LbL procedure to synthesize the MIL-103 (Eu(III), Tb(III), Gd(III)) in the form of a thin film is described in the Experimental Section. Film deposition on a functionalized substrate could be monitored in situ using a QCM, as shown in Figure 1c. The resulting thin films, also referred to as SURMOFs, of Eu(III), Tb(III), and Gd(III) exhibited similar out-of-plane diffraction patterns. The XRD data are fully consistent with patterns from simulations using the MIL-103 structure, demonstrating the presence of phase-pure isostructural MIL-103 for all three lanthanides used here (Figures 1b and S1).

The SURMOF infrared reflection absorption spectra (IRRAS) exhibited the characteristic asymmetric and symmetric stretching vibrations of the $-COO^-$ groups in the range of 1583−1528 and 1412−1375 cm^{-1}, respectively (Figure S2).[46] These data are fully consistent with the presence of [LnO_9] building units, a key structural motif of the MIL-103 structure. The stability of the SURMOFs after immersion in different solvents was checked by out-of-plane XRD experiments. The absence of immersion-induced changes reveals an exceptional solvent tolerance (Figure S3).

Using the LbL growth, continuous MIL-103 SURMOFs can be produced with controllable thickness and roughness. As shown in Figures 2a,b, and S4, scanning electron microscope (SEM) and atomic force microscope (AFM) images exhibited uniform surface coverage of MIL-103 SURMOFs on the

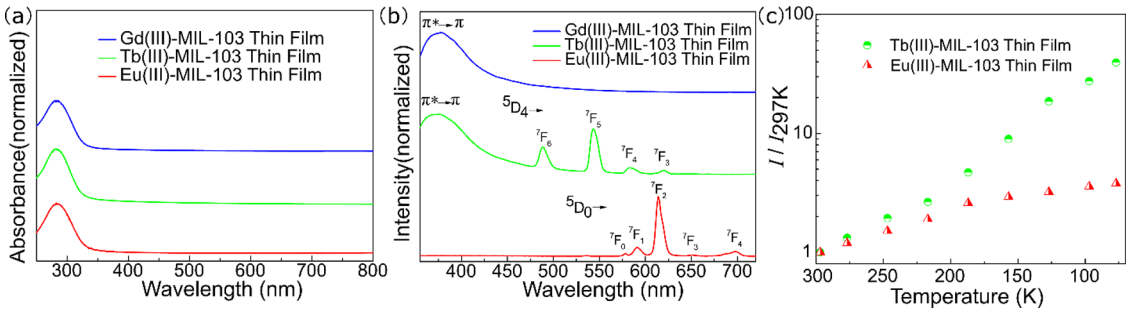

Figure 3. (a) UV−Vis absorbance spectra of Ln(III)-MIL-103 thin films (Ln = Eu(III), Tb(III) or Gd(III)); (b) emission spectra of Ln(III)-MIL-103 thin films (Ln = Eu(III), Tb(III) or Gd(III)); (c) ratio of intensity at different temperature (I) to the intensity at 297 K (I_{297K}) (green: Tb(III)-MIL-103 thin film; red: Eu(III)-MIL-103 thin film).

substrate. Unwanted light scattering effects from the surface were drastically reduced, thus avoiding a substantial loss of optical transparency. As illustrated in Figure 2c, the experimental data revealed that the transmittances of MIL-103 SURMOFs were beyond 92% (blank substrate as reference) in the visible light range.

We have studied the photophysical properties of the MIL-103 SURMOFs. For all three different MOF thin films, the absorbance spectra exhibited a maximum at 285 nm, corresponding to the $\pi-\pi^*$ transition of the linker BTB (Figure 3a). Upon excitation at 285 nm, the Eu(III) and Tb(III) MIL-103 thin films exhibited characteristic emission lines (Figure 3b). For Eu(III) MIL-103, the luminescence peaks were located at 578, 590, 614, 653, and 697 nm. These peaks are the result of transitions from the excited $^5D_0$ state to the ^7F_J (J = 0, 1, 2, 3, and 4) ground state.[46] The transition from $^5D_0$ to $^7F_2$ at 614 nm (red) exhibited the highest intensity. Tb(III) MIL-103 exhibited—in addition to the broad BTB $\pi^*-\pi$ emission at 384 nm, four sharp peaks at 489, 543, 584, and 616 nm, which are assigned to the transitions from the excited $^5D_4$ level to the ^7F_J (J = 6, 5, 4, and 3) ground state.[46] The peaks at 489 and 543 nm (green) are the most intense emissions. In the case of Gd(III) MIL-103 thin film, only the BTB based emission at 375 nm (Figure 3b) was observed. No emission from Gd(III)-states were observed since the excited state 4f levels of Gd(III) are located far above the triplet excited state of the antenna.[47,48] As noted above, direct excitation of Ln levels (i.e., without antenna effect) is so weak that it could not be observed in these experiments.

The well-resolved, intense emission peaks of Tb(III) and Eu(III)-based MIL-103 MOFs make them suitable for temperature-sensing applications, as demonstrated in the previous work.[10−12,19,35] Briefly, the temperature dependence of the emission intensities can be explained as follows.

The primary process is the absorption of UV light by the BTB ligand, leading to an excited triplet state. The energy is then transferred to the long-lived lanthanide resonance levels, from where re-emission takes place.[13−15,49] If the triplet-resonance energy gap (Δ_{EST}) is sufficiently small (<1850 cm^{-1}), the long lifetime of the excited Ln ions allows for a transfer back to the BTB triplet state.[49] Because of the activation energy needed, this back-transfer will be more efficient for higher temperatures. In the present case, Δ_{EST} for Eu(III) and Tb(III) MIL-103 SURMOFs amount to 3583 and 403 cm^{-1}, respectively (Figure S6). Hence, for Eu(III), the activation energy for the back-transfer is so large that the intensity will be very low for the temperature regime studied here.

This temperature dependence of the emission profiles recorded in the temperature range of 297−77 K is fully consistent with this expectation. Eu(III) showed only a weak temperature response compared to the Tb(III) MIL-103 film (Figures 3c and S6).

For the fabrication of SURMOF-based temperature sensors reported here, we employed three different strategies: (i) a mixed-layer Eu(III)-and-Tb(III) MIL-103 SURMOF; (ii) a bilayer hetero-SURMOF obtained by growing Eu(III) MIL-103 on top of Tb(III)-MIL-103; (iii) trilayer hetero-SURMOF obtained by growing Eu(III) MIL-103 on Gd(III) MIL-103 on Tb(III) MIL-103. While the first type of mixed-lanthanide structure can be easily made by the conventional solvothermal approach, the second and third approaches are only feasible by the LbL epitaxy approach, as described before. The three thin films prepared by these three approaches are denoted as $Eu_{3\%}/Tb_{97\%}$ mixed-layer, $Eu_{2cycle}/Tb_{65cycle}$-heterolayer, and $Eu_{2cycle}/Gd_{2cycle}/Tb_{65cycle}$-heterolayer. Figure 4a−c shows the entire emission spectra of the MOF thin films with changing temperature. Note that both of these films have a similar Eu(III):Tb(III) ratio, but exhibit different thermal responses, as illustrated Figure S7.

Using the emission lifetimes of the Tb(III) and Eu(III), for both of the thin films, a temperature-dependent energy transfer efficiency can be determined (see Figure S8). The energy transfer efficiency was calculated using the following equation:[11,50]

$$E = 1 - \frac{\tau_{Tb/Eu}}{\tau_{Tb}}$$

where $\tau_{Tb/Eu}$ and τ_{Tb} are the emission lifetime Tb(III) at 543 nm, in the presence and absence of Eu(III), respectively. Evidently, the $Eu_{3\%}/Tb_{97\%}$ mixed-layer SURMOF exhibited a substantially higher intra-ion energy transfer efficiency than the $Eu_{2cycle}/Tb_{65cycle}$-heterolayer, particularly at higher temperatures. Meanwhile, the energy transfer in the $Eu_{2cycle}/Tb_{65cycle}$-heterolayer was higher than in the $Eu_{2cycle}/Gd_{2cycle}/Tb_{65cycle}$-heterolayer. The steady increase of energy transfer efficiency with increasing temperature is attributed to the phonon-assisted Förster energy transfer mechanism.[51,52]

Commonly used figures of merit for temperature sensors are the thermometric parameter Δ and thermal sensitivity Sr, which are defined by:[8,28,53]

$$\Delta = \frac{I_{Tb543}}{I_{Eu614}} \quad S_r = \frac{1}{\Delta}\left|\frac{\partial \Delta}{\partial T}\right|$$

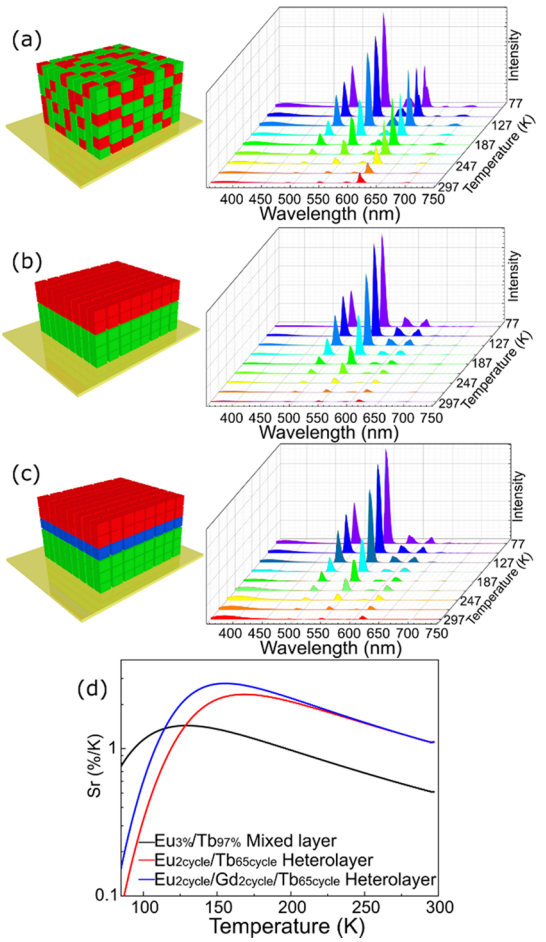

Figure 4. Schematic drawing and emission spectra of (a) $Eu_{3\%}/Tb_{97\%}$-BTB mixed-layer thin film; (b) heterolayer $Eu_{2cycle}/Tb_{65cycle}$-BTB thin film; (c) heterolayer $Eu_{2cycle}/Gd_{2cycle}/Tb_{65cycle}$-BTB thin film; Eu(III) are shown in red, Tb(III) are shown in green, and Gd(III) are shown in blue; (d) corresponding relative thermal sensitivity Sr of $Eu_{3\%}/Tb_{97\%}$-BTB mixed-layer thin film (black), heterolayer $Eu_{2cycle}/Tb_{65cycle}$-BTB thin film (red) and heterolayer $Eu_{2cycle}/Gd_{2cycle}/Tb_{65cycle}$-BTB thin film (blue).

where I_{Tb543} and I_{Eu614} are the intensities of the emission from $^5D_4$ to $^7F_5$ in Tb(III) at 543 nm and $^5D_0$ to $^7F_2$ in Eu(III) at 614 nm. As shown in Figure S9, for all SURMOF types, the thermometric parameter decreases with increasing temperature. The analogous temperature-dependent emission behavior can be mainly attributed to the obvious thermal response in the Tb(III) MIL-103. The Δ value is higher for the $Eu_{2cycle}/Tb_{65cycle}$-heterolayer and $Eu_{2cycle}/Gd_{2cycle}/Tb_{65cycle}$-heterolayer because the energy transfer from Tb(III) to Eu(III) is strongly reduced due to the larger average distance in these two heterolayer SURMOFs.

In both hetero- and homo-Eu(III)/Tb(III) MIL-103 SURMOF, the Δ value can be well-described by the classical Mott−Seitz model for a single nonradiative recombination channel.[8,9,17] When beyond 120 K, the uncontrollable Tb(III) to Eu(III) energy transfer hindered the weak radiative emission in the Tb(III) MIL-103. Therefore, the thermal response in hetero-SURMOF with controlled energy transfer showed better thermal sensitivity beyond the 120 K range. However, when the green emission from Tb(III) MIL-103 is dominant in radiative emission below 120 K (close to the Inflection point in the S-shaped curve), the reducing energy transfer led to higher radiative emission from Tb(III) MIL-103. Hence, the thermal sensitivity of homo-SURMOF performed better when below 120 K. The thermal sensitivity profiles revealed that different energy transfer efficiencies from Tb(III) to Eu(III) induce distinguishing better sensing range (Figure 4d). The hetero-SURMOF exhibited good sensing performance in the range of 120 K to room temperature. Combined with homo-SURMOF, MIL-103 thin film can be used as an excellent optical thermometer in the temperature regime from 77 K to room temperature, which is one of the common working ranges of cryogenics. The durability of the MIL-103 thin film was also exhibited by the revisable thermometric parameter between 77 and 297 K in Figure S10 and the XRD pattern after the thermal-response photoluminescence measurement in Figure S11. The better performance of the hetero-SURMOF over the homo-SURMOF can be directly visualized (see Figure 5). The

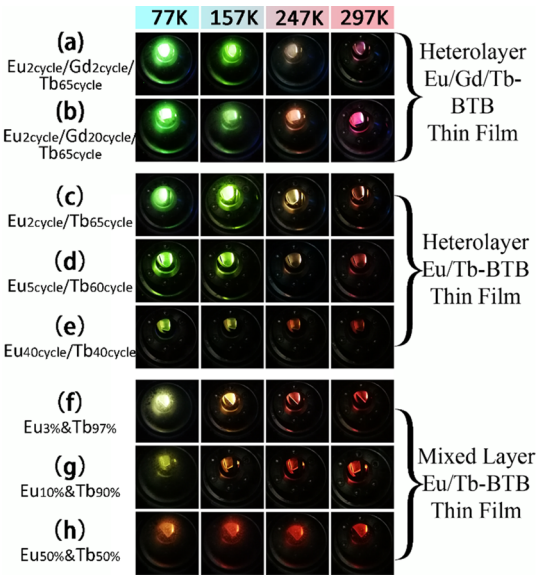

Figure 5. Optical photographs of (a) heterolayer $Eu_{2cycle}/Gd_{2cycle}/Tb_{65cycle}$-BTB thin film, (b) heterolayer $Eu_{2cycle}/Gd_{20cycle}/Tb_{65cycle}$-BTB thin film, (c) heterolayer $Eu_{2cycle}/Tb_{65cycle}$-BTB thin film, (d) heterolayer $Eu_{5cycle}/Tb_{60cycle}$-BTB thin film, (e) heterolayer $Eu_{40cycle}/Tb_{40cycle}$-BTB thin film, (f) $Eu_{3\%}/Tb_{97\%}$-BTB mixed-layer thin film, (g) $Eu_{10\%}/Tb_{90\%}$-BTB mixed-layer thin film and (h) $Eu_{50\%}/Tb_{50\%}$-BTB mixed-layer thin film under 285 nm excitation in 77, 157, 247, and 297 K.

performance is dependent on the photoluminescent nature of the nanoscale-thickness MIL-103 thin film; hence, the sensing speed is extremely fast compared with the changing speed of environment temperature. The photoluminescence quantum yields (PLQY) of homo- and hetero-MIL-103 thin films are shown in Table S2. For all the five different heterolayer MIL-103 MOFs, the emission color differences above 120 K are very distinct and can be seen by the naked eye (green, orange, red), in contrast to the mixed Eu(III)-and-Tb(IIII) MIL-103 thin film.

CONCLUSIONS

In summary, a series of luminescent, transparent, MIL-103 MOF thin films, or SURMOFs, based on Tb(III), Eu(III), and Gd(III) ions were synthesized by employing an LbL epitaxy method. The high transmittance of Ln(III)-SURMOFs can be achieved by precisely controlling the thickness and roughness

in the LbL approach. The hetero-SURMOFs consisting of Tb(III)−Eu(III) MIL-103 bilayer and Tb(III)-Gd(III)−Eu-(III) MIL-103 trilayer outperformed the mixed-MOF thin film as regards thermal sensitivity by about a factor of three in the temperature regime above 120 K. This pronounced increase of thermal sensitivity results from the heterolayer architecture, for which the average Tb-Eu distance is strongly increased, leading to a strong suppression of unwanted Tb(III)-Eu(III) energy transfer. This design approach can be used to design lanthanide-based luminescent thermometers with high efficiency. In the future also other LbL-based architectures will be used, e.g., for the fabrication of MOF-coated magnetic nanoparticles[54] suitable for temperature measurements in microfluidic channels.

EXPERIMENTAL SECTION

Fabrication of Tb(III)-MIL-103 Thin Film. Quartz glass substrates were rinsed with ethanol and dried in a stream of N_2 gas. Afterward, the quartz glass substrates were treated with oxygen plasma for 15 min to remove the impurities and increase the number of hydroxyl functional groups. Tb(III)-MIL-103 thin films were grown on the treated quartz glass substrate by the LbL approach at 65 °C. At first, the quartz glass was immersed in an ethanolic solution of $Tb(NO_3)_3$ (5×10^{-4} M) for 15 min. Afterward, the quartz glass was rinsed with pure ethanol twice and immersed into a 3×10^{-4} M ethanolic solution of BTB linker for 15 min. Then, the quartz glass was rinsed with pure ethanol again to remove the uncoordinated linker on the surface. This LbL growth process was repeated from 2 cycles to 100 cycles according to the required thickness.

Fabrication of Eu(III)-MIL-103 Thin Film. Similar to the fabrication of Tb(III)-MIL-103 thin film. Eu(III)-MIL-103 thin film was grown by the LbL approach with an ethanolic solution of $Eu(NO_3)_3$ (5×10^{-4} M) and BTB linker (3×10^{-4} M). The thickness was controlled by the process cycles of the LbL approach.

Fabrication of Doping Eu/Tb-BTB Thin Films. Quartz glass substrates were treated the same as the substrates used in Tb-BTB thin films. Then, doping Eu/Tb-BTB thin films were grown on the quartz glass substrate by the LbL approach at 65 °C as well. In the beginning, the quartz glass was immersed in an ethanolic solution of mixed $Eu(NO_3)_3$ and $Tb(NO_3)_3$ for 15 min. The total concentration of the ethanolic solution is 5×10^{-4} M and the ratio of $Eu(NO_3)_3$ and $Tb(NO_3)_3$ depend on the requirement of the samples. Afterward, the quartz glass was rinsed with pure ethanol twice and immersed in a 3×10^{-4} M ethanolic solution of the BTB linker for 15 min. Then, the quartz glass was rinsed with pure ethanol again to remove the uncoordinated linker on the surface. This LbL growth process was repeated from 2 cycles to 100 cycles according to the required thickness.

Fabrication of heterolayer Eu/Tb-BTB thin film: Quartz glass substrates were treated the same as the substrates used in Tb-BTB thin films. Then, Tb-BTB thin films were grown on the treated quartz glass substrate by the LbL approach at 65 °C at first. The quartz glass was immersed in an ethanolic solution of $Tb(NO_3)_3$ (5×10^{-4} M) for 15 min. Afterward, the quartz glass was rinsed with pure ethanol twice and immersed in a 3×10^{-4} M ethanolic solution of BTB linker for 15 min. Then, the quartz glass was rinsed with pure ethanol again to remove the uncoordinated linker on the surface. This LbL growth process was repeated from 2 cycles to 100 cycles according to the required thickness of Tb-SURMOFs. After the growth of Tb-BTB thin film, the samples were immersed in an ethanolic solution of $Eu(NO_3)_3$ (5×10^{-4} M) and the same fabricating process of Eu-BTB thin film started immediately. The ratio of Eu(III) and Tb(III) was controlled by the growth layers of each material in the LbL process.

Fabrication of heterolayer Eu/Gd/Tb-BTB thin film: Similar to the fabrication of heterolayer Eu/Tb-BTB thin film, the samples were immersed in an ethanolic solution of $Gd(NO_3)_3$ (5×10^{-4} M) and BTB linker (3×10^{-4} M) for LbL growth between the growth of Tb(III)-MIL-103 and Eu(III)-MIL-103.

AUTHOR INFORMATION

Corresponding Author

Dong-Hui Chen − *Institute of Functional Interfaces (IFG), Karlsruhe Institute of Technology (KIT), Eggenstein-Leopoldshafen 76344, Germany;* orcid.org/0000-0003-2561-2444; Email: donghui.chen@kit.edu

Authors

Ritesh Haldar − *Tata Institute of Fundamental Research, Hyderabad, Telangana 500046, India;* orcid.org/0000-0001-9697-9169

Christof Wöll − *Institute of Functional Interfaces (IFG), Karlsruhe Institute of Technology (KIT), Eggenstein-Leopoldshafen 76344, Germany;* orcid.org/0000-0003-1078-3304

Notes

The authors declare no competing financial interest.

ACKNOWLEDGMENTS

C.W. acknowledges support through the Deutsche Forschungsgemeinschaft (DFG) within the Cluster "3DMM2O" funded by Germany's Excellence Strategy—2082/1-390761711. R.H. acknowledges intramural funds at TIFR Hyderabad from the Department of Atomic Energy (DAE), India, under Project Identification Number RTI 4007. The authors also would like to thank Ling Lin for technical assistance on the SEM measurements.

REFERENCES

(1) Chen, K.; Yao, L.; Su, B. Bionic Thermoelectric Response with Nanochannels. *J. Am. Chem. Soc.* **2019**, *141*, 8608−8615.

(2) Stich, M. I.; Fischer, L. H.; Wolfbeis, O. S. Multiple Fluorescent Chemical Sensing and Imaging. *Chem. Soc. Rev.* **2010**, *39*, 3102−3114.

(3) Shen, Q.; Luo, Z.; Ma, S.; Tao, P.; Song, C.; Wu, J.; Shang, W.; Deng, T. Bioinspired Infrared Sensing Materials and Systems. *Adv. Mater.* **2018**, *30*, No. 1707632.

(4) Meng, L.; Jiang, S.; Song, M.; Yan, F.; Zhang, W.; Xu, B.; Tian, W. TICT-Based near-Infrared Ratiometric Organic Fluorescent Thermometer for Intracellular Temperature Sensing. *ACS Appl. Mater. Interfaces* **2020**, *12*, 26842−26851.

(5) Wang, J.; Zakrzewski, J. J.; Heczko, M.; Zychowicz, M.; Nakagawa, K.; Nakabayashi, K.; Sieklucka, B.; Chorazy, S.; Ohkoshi, S. Proton Conductive Luminescent Thermometer Based on Near-Infrared Emissive $\{YbCo_2\}$ Molecular Nanomagnets. *J. Am. Chem. Soc.* **2020**, *142*, 3970−3979.

(6) Manzani, D.; Petruci, J. F.; Nigoghossian, K.; Cardoso, A. A.; Ribeiro, S. J. A Portable Luminescent Thermometer Based on Green Up-Conversion Emission of Er^{3+}/Yb^{3+} Co-Doped Tellurite Glass. *Sci. Rep.* **2017**, *7*, 41596.

(7) Wang, H.; Yao, Y.; He, Z.; Rao, W.; Hu, L.; Chen, S.; Lin, J.; Gao, J.; Zhang, P.; Sun, X.; Wang, X.; Cui, Y.; Wang, Q.; Dong, S.; Chen, G.; Liu, J. A Highly Stretchable Liquid Metal Polymer as

Reversible Transitional Insulator and Conductor. *Adv. Mater.* **2019**, *31*, No. 1901337.
(8) Wang, Z.; Ananias, D.; Carné-Sánchez, A.; Brites, C. D.; Imaz, I.; Maspoch, D.; Rocha, J.; Carlos, L. D. Lanthanide−Organic Framework Nanothermometers Prepared by Spray-Drying. *Adv. Funct. Mater.* **2015**, *25*, 2824−2830.
(9) Li, Y. Temperature and Humidity Sensors Based on Luminescent Metal-Organic Frameworks. *Polyhedron* **2020**, *179*, No. 114413.
(10) Cui, Y.; Xu, H.; Yue, Y.; Guo, Z.; Yu, J.; Chen, Z.; Gao, J.; Yang, Y.; Qian, G.; Chen, B. A Luminescent Mixed-Lanthanide Metal−Organic Framework Thermometer. *J. Am. Chem. Soc.* **2012**, *134*, 3979−3982.
(11) Thapa, K. B.; Chen, B.; Bian, L.; Xu, Y.; He, J.; Huang, W.; Ju, Q.; Fang, Z. Single-Metallic Thermoresponsive Coordination Network as a Dual-Parametric Luminescent Thermometer. *ACS Appl. Mater. Interfaces* **2021**, *13*, 35905−35913.
(12) Wang, S.; Zhang, J.; Wu, J.; Ye, Z.; Yu, H.; Zhang, H. Rational Design of a Nd^{3+}-Mn^{4+} Co-doped Luminescent Thermometer: Towards High-Sensitivity Temperature Sensing. *ChemPhotoChem* **2021**, *5*, 455−465.
(13) Yin, H.-Q.; Wang, X.-Y.; Yin, X.-B. Rotation Restricted Emission and Antenna Effect in Single Metal−Organic Frameworks. *J. Am. Chem. Soc.* **2019**, *141*, 15166−15173.
(14) Pan, M.; Liao, W.-M.; Yin, S.-Y.; Sun, S.-S.; Su, C.-Y. Single-Phase White-Light-Emitting and Photoluminescent Color-Tuning Coordination Assemblies. *Chem. Rev.* **2018**, *118*, 8889−8935.
(15) Chen, D.-H.; Lin, L.; Sheng, T.-L.; Wen, Y.-H.; Zhu, X.-Q.; Zhang, L.-T.; Hu, S.-M.; Fu, R.-B.; Wu, X.-T. Syntheses, Structures, Luminescence and Magnetic Properties of Seven Isomorphous Metal−Organic Frameworks Based on 2, 7-Bis (4-Benzoic Acid)-N-(4-Benzoic Acid) Carbazole. *New J. Chem.* **2018**, *42*, 2830−2837.
(16) Chen, Q.; Liu, Q.; Chen, J.; Wang, L.; Ma, X.; Zhang, Z.; Xiang, S. Metal Organic Frameworks Composite Eu_2O_3@[Zn_2(1,4-Ndc)$_2$dabco] Synthesized by Pulsed Laser Ablation in Flowing Liquid and Its Fluorescent Sensing of Fatty Alcohol with Different Branch Chains. *Opt. Mater.* **2020**, *105*, No. 109886.
(17) Ding, Y.; Lu, Y.; Yu, K.; Wang, S.; Zhao, D.; Chen, B. MOF-Nanocomposite Mixed-Matrix Membrane for Dual-Luminescence Ratiometric Temperature Sensing. *Adv. Opt. Mater.* **2021**, *9*, No. 2100945.
(18) Yang, X.; Zou, H.; Sun, X.; Sun, T.; Guo, C.; Fu, Y.; Wu, C. L.; Qiao, X.; Wang, F. One-Step Synthesis of Mixed Lanthanide Metal−Organic Framework Films for Sensitive Temperature Mapping. *Adv. Opt. Mater.* **2019**, *7*, No. 1900336.
(19) Rocha, J.; Brites, C. D.; Carlos, L. D. Lanthanide Organic Framework Luminescent Thermometers. *Chem. − Eur. J.* **2016**, *22*, 14782−14795.
(20) Binnemans, K. Lanthanide-Based Luminescent Hybrid Materials. *Chem. Rev.* **2009**, *109*, 4283−4374.
(21) Latva, M.; Takalo, H.; Mukkala, V.-M.; Matachescu, C.; Rodríguez-Ubis, J. C.; Kankare, J. Correlation between the Lowest Triplet State Energy Level of the Ligand and Lanthanide (III) Luminescence Quantum Yield. *J. Lumin.* **1997**, *75*, 149−169.
(22) Liu, L.; Chen, Y.; Yao, Z.; Chen, D.; Lin, Q.; Fan, Z.; Zhang, Z.; Chen, B.; Xiang, S. Two Tb-Metal Organic Frameworks with Different Metal Cluster Nodes for C_2 H_2/CO_2 Separation. *Dalton Trans.* **2021**, *50*, 4932−4935.
(23) Miyata, K.; Konno, Y.; Nakanishi, T.; Kobayashi, A.; Kato, M.; Fushimi, K.; Hasegawa, Y. Chameleon Luminophore for Sensing Temperatures: Control of Metal-to-metal and Energy Back Transfer in Lanthanide Coordination Polymers. *Angew. Chem., Int. Ed.* **2013**, *52*, 6413−6416.
(24) Li, L.; Zhu, Y.; Zhou, X.; Brites, C. D.; Ananias, D.; Lin, Z.; Paz, F. A. A.; Rocha, J.; Huang, W.; Carlos, L. D. Visible-light Excited Luminescent Thermometer Based on Single Lanthanide Organic Frameworks. *Adv. Funct. Mater.* **2016**, *26*, 8677−8684.
(25) Wang, H.; Zhao, D.; Cui, Y.; Yang, Y.; Qian, G. A Eu/Tb-Mixed MOF for Luminescent High-Temperature Sensing. *J. Solid State Chem.* **2017**, *246*, 341−345.
(26) Xia, T.; Cao, W.; Guan, L.; Zhang, J.; Jiang, F.; Yu, L.; Wan, Y. Three Isostructural Hexanuclear Lanthanide−Organic Frameworks for Sensitive Luminescence Temperature Sensing over a Wide Range. *Dalton Trans.* **2022**, *51*, 5426−5433.
(27) Feng, T.; Ye, Y.; Liu, X.; Cui, H.; Li, Z.; Zhang, Y.; Liang, B.; Li, H.; Chen, B. A Robust Mixed-lanthanide PolyMOF Membrane for Ratiometric Temperature Sensing. *Angew. Chem., Int. Ed.* **2020**, *59*, 21752−21757.
(28) Kaczmarek, A. M.; Liu, Y.; Kaczmarek, M. K.; Liu, H.; Artizzu, F.; Carlos, L. D.; Van Der Voort, P. Developing Luminescent Ratiometric Thermometers Based on a Covalent Organic Framework (COF). *Angew. Chem., Int. Ed.* **2020**, *59*, 1932−1940.
(29) Zhou, J.; Zheng, G.; Liu, X.; Dong, G.; Qiu, J. Defect Engineering in Lanthanide Doped Luminescent Materials. *Coord. Chem. Rev.* **2021**, *448*, No. 214178.
(30) Allendorf, M. D.; Bauer, C. A.; Bhakta, R.; Houk, R. Luminescent Metal−Organic Frameworks. *Chem. Soc. Rev.* **2009**, *38*, 1330−1352.
(31) Sánchez-González, E.; Tsang, M. Y.; Troyano, J.; Craig, G. A.; Furukawa, S. Assembling Metal−Organic Cages as Porous Materials. *Chem. Soc. Rev.* **2022**, *51*, 4876−4889.
(32) Cui, Y.; Zou, W.; Song, R.; Yu, J.; Zhang, W.; Yang, Y.; Qian, G. A Ratiometric and Colorimetric Luminescent Thermometer over a Wide Temperature Range Based on a Lanthanide Coordination Polymer. *Chem. Commun.* **2014**, *50*, 719−721.
(33) Pan, Y.; Su, H.-Q.; Zhou, E.-L.; Yin, H.-Z.; Shao, K.-Z.; Su, Z.-M. A Stable Mixed Lanthanide Metal−Organic Framework for Highly Sensitive Thermometry. *Dalton Trans.* **2019**, *48*, 3723−3729.
(34) Haldar, R.; Mazel, A.; Krstić, M.; Zhang, Q.; Jakoby, M.; Howard, I. A.; Richards, B. S.; Jung, N.; Jacquemin, D.; Diring, S.; Wenzel, W.; Odobel, F.; Wöll, C. A de Novo Strategy for Predictive Crystal Engineering to Tune Excitonic Coupling. *Nat. Commun.* **2019**, *10*, 2048.
(35) Liu, J.; Pei, L.; Xia, Z.; Xu, Y. Hierarchical Accordion-like Lanthanide-Based Metal−Organic Frameworks: Solvent-Free Syntheses and Ratiometric Luminescence Temperature-Sensing Properties. *Cryst. Growth Des.* **2019**, *19*, 6586−6591.
(36) Sahoo, S.; Mondal, S.; Sarma, D. Luminescent Lanthanide Metal Organic Frameworks (LnMOFs): A Versatile Platform towards Organomolecule Sensing. *Coord. Chem. Rev.* **2022**, *470*, No. 214707.
(37) Wu, S.; Lin, Y.; Liu, J.; Shi, W.; Yang, G.; Cheng, P. Rapid Detection of the Biomarkers for Carcinoid Tumors by a Water Stable Luminescent Lanthanide Metal−Organic Framework Sensor. *Adv. Funct. Mater.* **2018**, *28*, No. 1707169.
(38) Santos, J. C.; Pramudya, Y.; Krstic, M.; Chen, D.-H.; Neumeier, B. L.; Feldmann, C.; Wenzel, W.; Redel, E. Halogenated Terephthalic Acid "Antenna Effects" in Lanthanide-SURMOF Thin Films. *ACS Appl. Mater. Interfaces* **2020**, *12*, 52166−52174.
(39) Haldar, R.; Wöll, C. Hierarchical Assemblies of Molecular Frameworks—MOF-on-MOF Epitaxial Heterostructures. *Nano Res.* **2021**, *14*, 355−368.
(40) Liu, J.; Wöll, C. Surface-Supported Metal−Organic Framework Thin Films: Fabrication Methods, Applications, and Challenges. *Chem. Soc. Rev.* **2017**, *46*, 5730−5770.
(41) Chen, D.; Haldar, R.; Neumeier, B. L.; Fu, Z.; Feldmann, C.; Wöll, C.; Redel, E. Tunable Emission in Heteroepitaxial Ln-SURMOFs. *Adv. Funct. Mater.* **2019**, *29*, No. 1903086.
(42) Chen, D.; Sedykh, A. E.; Gomez, G. E.; Neumeier, B. L.; Santos, J. C.; Gvilava, V.; Maile, R.; Feldmann, C.; Wöll, C.; Janiak, C.; Müller-Buschbaum, K.; Redel, E. SURMOF Devices Based on Heteroepitaxial Architectures with White-Light Emission and Luminescent Thermal-Dependent Performance. *Adv. Mater. Interfaces* **2020**, *7*, No. 2000929.
(43) Devic, T.; Serre, C.; Audebrand, N.; Marrot, J.; Férey, G. MIL-103, a 3-D Lanthanide-Based Metal Organic Framework with Large

One-Dimensional Tunnels and a High Surface Area. *J. Am. Chem. Soc.* **2005**, *127*, 12788−12789.
(44) Duan, J.; Higuchi, M.; Horike, S.; Foo, M. L.; Rao, K. P.; Inubushi, Y.; Fukushima, T.; Kitagawa, S. High CO_2/CH_4 and C_2 Hydrocarbons/CH_4 Selectivity in a Chemically Robust Porous Coordination Polymer. *Adv. Funct. Mater.* **2013**, *23*, 3525−3530.
(45) Ugale, B.; Dhankhar, S. S.; Nagaraja, C. Exceptionally Stable and 20-Connected Lanthanide Metal−Organic Frameworks for Selective CO_2 Capture and Conversion at Atmospheric Pressure. *Cryst. Growth Des.* **2018**, *18*, 2432−2440.
(46) Hadjiivanov, K. I.; Panayotov, D. A.; Mihaylov, M. Y.; Ivanova, E. Z.; Chakarova, K. K.; Andonova, S. M.; Drenchev, N. L. Power of Infrared and Raman Spectroscopies to Characterize Metal-Organic Frameworks and Investigate Their Interaction with Guest Molecules. *Chem. Rev.* **2021**, *121*, 1286−1424.
(47) Belousov, Y. A.; Drozdov, A. A.; Taydakov, I. V.; Marchetti, F.; Pettinari, R.; Pettinari, C. Lanthanide Azolecarboxylate Compounds: Structure, Luminescent Properties and Applications. *Coord. Chem. Rev.* **2021**, *445*, No. 214084.
(48) Li, Z.; Wang, G.; Ye, Y.; Li, B.; Li, H.; Chen, B. Loading Photochromic Molecules into a Luminescent Metal−Organic Framework for Information Anticounterfeiting. *Angew. Chem., Int. Ed.* **2019**, *58*, 18025−18031.
(49) Heine, J.; Müller-Buschbaum, K. Engineering Metal-Based Luminescence in Coordination Polymers and Metal−Organic Frameworks. *Chem. Soc. Rev.* **2013**, *42*, 9232−9242.
(50) Zhou, Y.; Yan, B. Lanthanides Post-Functionalized Nanocrystalline Metal−Organic Frameworks for Tunable White-Light Emission and Orthogonal Multi-Readout Thermometry. *Nanoscale* **2015**, *7*, 4063−4069.
(51) Liu, Y.; Qian, G.; Wang, Z.; Wang, M. Temperature-Dependent Luminescent Properties of Eu−Tb Complexes Synthesized in Situ in Gel Glass. *Appl. Phys. Lett.* **2005**, *86*, No. 071907.
(52) Ananias, D.; Kostova, M.; Almeida Paz, F. A.; Ferreira, A.; Carlos, L. D.; Klinowski, J.; Rocha, J. Photoluminescent Layered Lanthanide Silicates. *J. Am. Chem. Soc.* **2004**, *126*, 10410−10417.
(53) Chen, C.; Zhuang, Y.; Li, X.; Lin, F.; Peng, D.; Tu, D.; Xie, A.; Xie, R. Achieving Remote Stress and Temperature Dual-modal Imaging by Double-lanthanide-activated Mechanoluminescent Materials. *Adv. Funct. Mater.* **2021**, *31*, No. 2101567.
(54) Silvestre, M. E.; Franzreb, M.; Weidler, P. G.; Shekhah, O.; Wöll, C. Magnetic Cores with Porous Coatings: Growth of Metal-Organic Frameworks on Particles Using Liquid Phase Epitaxy. *Adv. Funct. Mater.* **2013**, *23*, 1210−1213.